Polarization Image Sensor for Highly Sensitive Polarization Modulation Imaging Based on Stacked Polarizers

Kiyotaka Sasagawa, *Member, IEEE*, Ryoma Okada, *Graduate Student Member, IEEE*, Makito Haruta, Hironari Takehara, *Member, IEEE*, Hiroyuki Tashiro, *Member, IEEE*, and Jun Ohta, *Fellow, IEEE*

***Abstract*— In this article, We demonstrated an image sensor for detecting changes in polarization with high sensitivity. For this purpose, we constructed an optical system with a two-layer structure, comprising an external polarizer and polarizers on a pixel array. An external polarizer is used to enhance the polarization rotation while reducing the intensity to avoid pixel saturation of the image sensor. Using a two-layer structure, the two polarizers can be arranged under optimal conditions and the image sensor can achieve high polarization-change detection performance. We fabricated the polarization image sensor using a 0.35-μm CMOS process and, by averaging 50 $\times$ 50 pixels and 96 frames, achieved a polarization rotation detection limit of 5.2 $\times$ 10^{-4° at a wavelength of 625 nm. We also demonstrated the applicability of electric-field distribution imaging using an electrooptic crystal (ZnTe) for weak-polarization-change distribution measurements.**

***Index Terms*— CMOS image sensor, electric-field imaging, ON-chip polarizer, polarization image sensor, polarization modulation imaging.**

I. Introduction

OPTICAL polarization detection can provide information that cannot be obtained by ordinary light intensity detection, such as the angle of the incident surface [1], differences in materials [2], distortions in a transparent material [3], and separation of reflected and transmitted components in transparent media. Image sensors have been proposed to image the distribution of polarization characteristics and have been realized using various polarizer materials.

Polarizers mounted on pixels have been developed to realize polarization imaging in image sensors. Polarization polymers [4], liquid crystals [5], photonic crystals [6], and metal wire grids [7]–[14] are some of the materials used. Recent years have seen the realization of polarizers and pixels mounted on them.

However, an image sensor presents limitations from the perspective of weak polarization modulation or polarization rotation measurement. When a different polarizer is placed in each pixel, it is difficult to achieve a high extinction ratio, unlike a single polarizer. In addition, to achieve a high signal-to-noise ratio (SNR), it is necessary to irradiate light with relatively high intensity so that the photon shot noise becomes dominant. However, this quickly saturates the small pixels of the image sensor to reach the limit. These limitations result in low polarization sensitivity compared to systems with discrete PDs, where the light source intensity can be sufficiently high. Therefore, there are some methods—based on highly sensitive polarization modulation measurements—in which it is difficult to apply an image sensor. Examples include the measurement of optical isomer concentrations in microfluidic channels [8] and high-frequency electric-field measurements of microwaves, millimeter waves, and terahertz waves using electrooptic (EO) crystals [15], [16]. In our previous works, we developed image sensors to observe small polarization changes in the range below 1°. However, further performance improvements are required.

To address these issues, we designed and fabricated a polarization image sensor with an ON-pixel polarizer and proposed a method for imaging small polarization modulation by constructing a multilayer polarizer, comprising an external polarizer and ON-pixel polarizers [17]. In a previous study, we detected weak polarization changes of $2.5 \times 10^{-3^\circ}$. In this study, we designed and fabricated a pixel with an MOS capacitor between pixels to further improve performance, reduce crosstalk, and increase pixel capacity for a higher SNR. As a result, the polarization-change detection performance of $5.2 \times 10^{-4^\circ}$ was achieved. We also demonstrated the feasibility of electric-field imaging using the proposed sensor and a (100)-ZnTe crystal.

Manuscript received October 29, 2021; accepted December 21, 2021. Date of publication January 28, 2022; date of current version May 24, 2022. This work was supported in part by JSPS KAKENHI under Grant JP21H03809 and in part by the Activities of VDEC, The University of Tokyo, in collaboration with the Cadence Design System and Mentor Graphics Corporation. The review of this article was arranged by Editor R. Kuroda. *(Corresponding author: Kiyotaka Sasagawa.)*

Kiyotaka Sasagawa, Ryoma Okada, Makito Haruta, Hironari Takehara, and Jun Ohta are with the Division of Materials Science, Graduate School of Science and Technology, Nara Institute of Science and Technology, Ikoma 630-0192, Japan (e-mail: sasagawa@ms.naist.jp; okada.ryoma.on9@ms.naist.jp; m-haruta@ms.naist.jp; t-hironari@ms.naist.jp; ohta@ms.naist.jp).

Hiroyuki Tashiro is with the Division of Medical Technology, Department of Health Sciences, Faculty of Medical Sciences, Kyushu University, Fukuoka 812-8582, Japan, and also with the Division of Materials Science, Graduate School of Science and Technology, Nara Institute of Science and Technology, Ikoma 630-0192, Japan (e-mail: htashiro@med.kyushu-u.ac.jp).

Color versions of one or more figures in this article are available at https://doi.org/10.1109/TED.2022.3140288.

Digital Object Identifier 10.1109/TED.2022.3140288

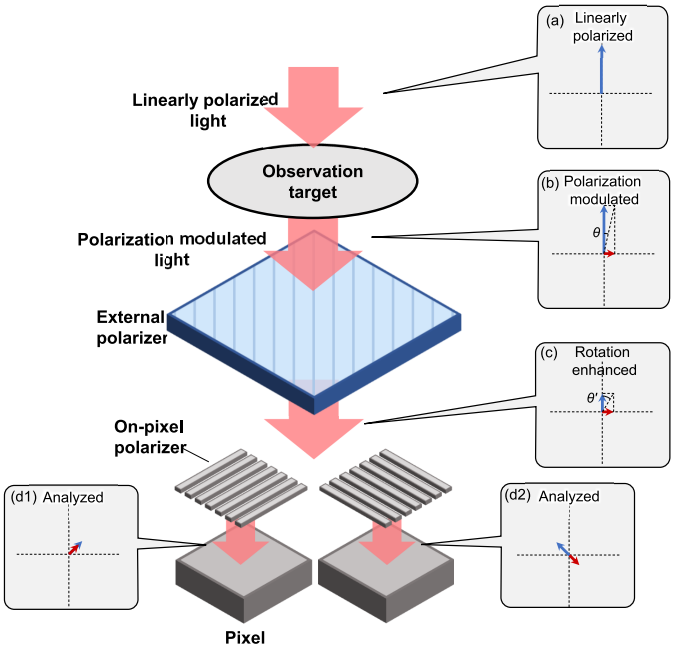

Fig. 1. Schematic of high-sensitivity polarization modulation detection using a multilayer polarizer structure.

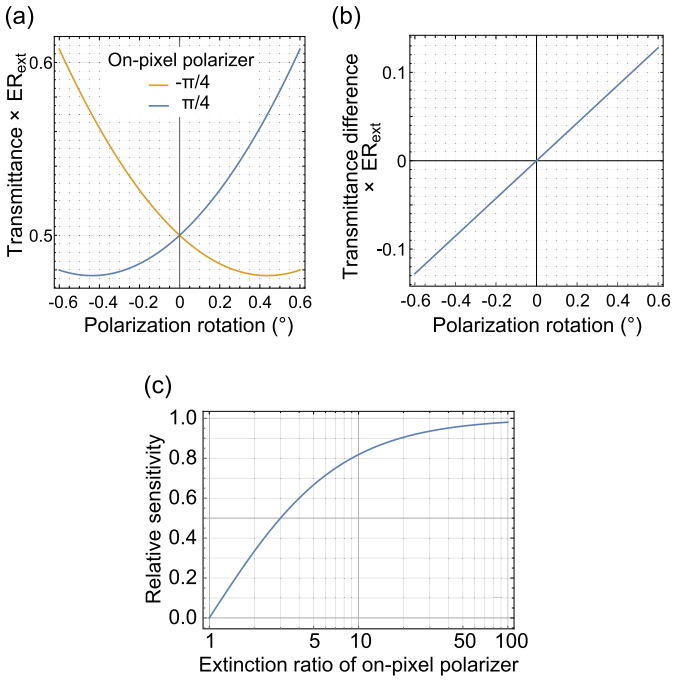

Fig. 2. (a) Theoretical transmittance curves of stacked polarizers. (b) Transmittance difference between $\pm\pi/4$-rad pixels. (c) Relative sensitivity as a function of the extinction ratio of on-chip polarizers. ER_{ext}: extinction ratio of the external polarizer.

In Section II, the functions of stacked polarizers are explained. In Section III, the design and characteristics of an image sensor with ON-pixel polarizers are described. In Section IV, to demonstrate small polarization modulation detection, an electric-field imaging system based on the electrooptic effect is constructed and the electric field on a microstrip line is imaged. In Section V, the characteristics of the proposed system are discussed. Conclusions are presented in Section VI.

II. Stacked Polarizer Configuration for Highly Sensitive Polarization Modulation Measurement by Image Sensor

A two-layer polarizer structure consisting of a top-pixel polarizer array and uniform polarizer was used for highly sensitive polarization-change detection. When detecting changes in polarization, a polarizer is commonly used as an analyzer for obtaining polarization rotation information by a photodetector. The highest sensitivity was achieved when the transmittance change was the largest for incident polarization. The polarizer was placed at an angle of $\pm 45°$ or $\pm\pi/4$ rad to the incident polarization. However, under these conditions, approximately half of the incident light is transmitted. This transmittance is unsuitable for image sensors because of its low-light saturation characteristics.

In contrast, the proposed method utilizes a configuration of two layers of polarizers, as shown in Fig. 1. The first layer is an external polarizer, which can achieve a high extinction ratio of 10^{-3} or higher, even with a polarizing beam splitter or a relatively inexpensive film polarizer. This polarizer is placed at an angle that blocks incident polarized light. When linearly polarized light is irradiated on an observation target, the polarization is slightly rotated. The output light can be described as a composite of components parallel and perpendicular to the incident polarization [Fig. 1(b)]. Here, the actual polarizer does not completely block the impermeable polarization component (the component parallel to the incident polarization) but transmits a small amount. In the proposed technique, the transmitted component is effectively used. However, most components generated by the polarization rotation caused by the observation target are transmitted through the external polarizer. The transmitted composite components are shown in Fig. 1(c). With this method, the polarization rotation angle can be enhanced while the light intensity is reduced. This effect enables the image sensor to detect weak polarization with higher sensitivity, despite its limited light-receiving capacity.

As mentioned above, the polarizer on the pixel acts as an analyzer for detecting the polarization signal, whose polarization rotation is enhanced by the external polarizer. These ON-pixel polarizers were placed at angles of $\pm\pi/4$ rad to the incident polarization. The light intensity transmitted through the proposed stacked polarizers was calculated and is plotted in Fig. 2(a). Here, the extinction ratios of the external polarizer and ON-pixel polarizer were set to 800 and 1.55, respectively. The differences between the two curves are presented in Fig. 2(b). This result indicates that the difference is almost proportional to the polarization rotation. In this way, the two polarizers, the external polarizer, and the ON-pixel polarizer contribute to enhancing the rotation angle and analyzing the polarized light, respectively. The polarizers can be optimally arranged to fulfill each role. The external polarizer enhances the angular change by reducing components other than those modulated by the observation target. By arranging

the ON-pixel polarizing element at $\pm\pi/4$ rad with respect to the incident polarized light, the polarization rotation is efficiently converted into intensity.

It is noted that the required extinction ratio of the ON-pixel polarizer is relatively low when polarizers are used as analyzers. It is difficult to obtain a high extinction ratio in a polarization image sensor, wherein polarizers with different polarization angles are placed in each pixel. Although recent research has led to an improved arrangement, the extinction ratio is still lower than that of uniform polarizers. In the proposed method, the ON-pixel polarizer was only used as an optical analyzer. Here, we assume that the ideal polarizers are located on the pixels. When the polarization change is converted to light intensity by the analyzer, the transmittance change $dT_{\text{onpix}}/d\theta$ is expressed as follows:

$$T_{\text{onpix}} = (\sin\theta)^2 \tag{1}$$

$$dT_{\text{onpix}}/d\theta = 2\sin\theta\cos\theta = \sin 2\theta \tag{2}$$

where T_{onpix} is the intensity transmittance and θ is the polarization angle of the incident light. When a polarizer is used as an analyzer, the optimum point is that at which the transmittance change reaches a maximum in response to polarization rotation; i.e., the point where the polarization angle can be written as $(1+2m)\pi/4$ rad, where m is an integer. In the case of $\pm\pi/4$ rad, m is 0 and -1. The polarization sensitivity increased as the extinction ratio increased. However, the improvement rate decreased as the extinction ratio increased. Fig. 2(c) shows the relative sensitivity as a function of the extinction ratio of on-chip polarizers. Here, we assume that the relative sensitivity is unity when the polarizer on the pixel is ideal, with an infinite extinction ratio. At an extinction ratio of 3, the relative sensitivity is approximately 0.5 and reaches 0.8 or higher at an extinction ratio of 10.

In contrast, the sensitivity improvement rate with the first external polarizer is given by $1/(T_\perp)^{1/2}$, where $T_\perp$ is the lowest intensity transmittance of the external polarizer. If the light source intensity can be sufficiently high, a higher polarization detection sensitivity is expected using a polarizer with a higher extinction ratio.

III. Image Sensor With On-Pixel Polarizers

The proposed method enables highly sensitive polarization-modulation detection using a polarization image sensor with a relatively low-performance ON-pixel polarizer. To demonstrate this, we designed a sensor chip using a 0.35-μm standard CMOS process. Table I lists the specifications of the chip. The overall picture and block diagram of the chip are shown in Fig. 3(a) and (b), respectively.

A. Pixel Design

Fig. 4(a) shows the pixel layout. To maintain low crosstalk, we adopted a large pixel spacing. In the present sensor, the pixel pitch was 30 μm while the photodiode (PD) in the pixel is 15 μm $\times$ 15 μm^2. The PD was surrounded by n-well guard rings pulled up to the supply voltage to reduce crosstalk between pixels.

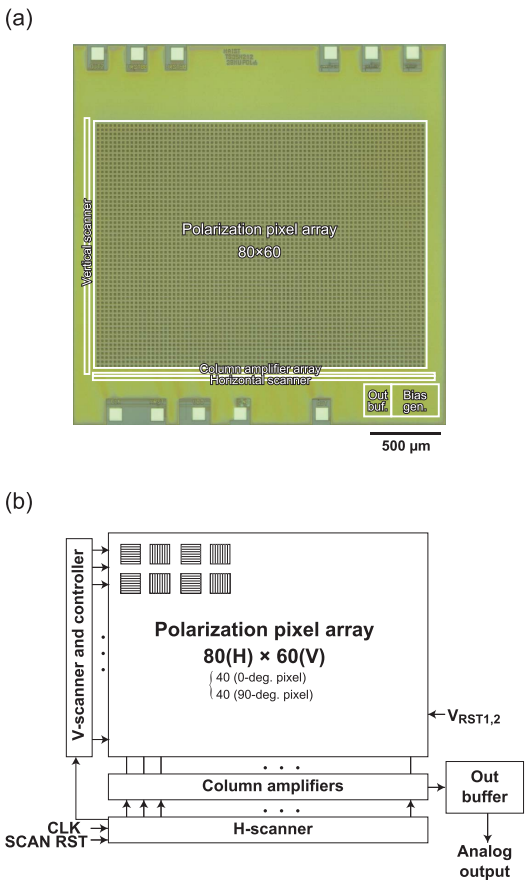

Fig. 3. (a) Photograph of the fabricated image sensor chip. (b) Block diagram.

TABLE I
Image Sensor Chip Specifications

Process	0.35-μm 2-poly 4-metal standard CMOS
Supply voltage	3.3 V
Pixel size	30 μm $\times$ 30 μm
Photodiode	n-well/p-sub
Photodiode size	15 μm $\times$ 15 μm
Fill factor	25%
Full well capacity	8 Me$^-$
Pixel type	3-Transistor active pixel sensor
Number of pixels	80 $\times$ 60
Maximum SNR	63 dB
On-chip polarizer	Line/Space = 0.5 μm / 0.45 μm 0° or 90°
Extinction ratio	1.55(0°), 1.53(90°) at 625 nm
Chip size	2.70 mm $\times$ 2.65 mm

A pixel-layout circuit diagram is shown in Fig. 4(b). A pMOS capacitance was placed in the n-well guard ring and connected to the PD. This layout makes it possible to effectively use the area between PDs. By increasing the pixel capacitance, the optical saturation limit increased and the maximum SNR improved. As mentioned previously, a stacked polarizer enhances the polarization rotation. Here, the high extinction ratio of the external polarizer narrows the angle range that can be measured. However, this effect would not be a problem when measuring the weak polarization modulation.

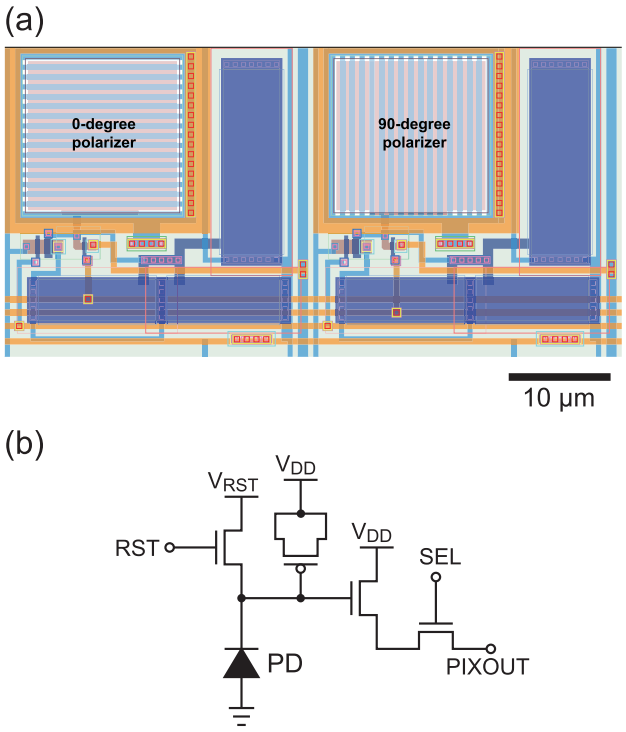

Fig. 4. (a) Layout of the polarization pixel pair. (b) Diagram of the pixel circuit.

Theoretically, as both the polarizer extinction ratio and light source increase, the polarization sensitivity increases. The practical light source intensity is several tens to hundreds of milliwatts. This value is very large compared to the saturated light amount of a general image sensor. Therefore, increasing the pixel capacity is also acceptable for improving the total performance.

The ON-pixel polarizer was composed of the metal wiring layer of the CMOS process, as in previous chips [17]. The line and space were 0.5 and 0.45 μm, respectively. Because this value is larger than the wavelength, the polarization transmission is different from that of nanostructured polarizers. As a result, the polarization component parallel to the grid showed a higher transmittance than that perpendicular to the grid.

The polarizer angles in the proposed image sensor were 0° and 90° because the polarizer on the pixel was used as an analyzer. Each column is equipped with only one type of polarizer, which facilitates signal processing at the column level. The external polarizer and these polarizers are arranged such that the transmission axes are at an angular difference of 45° from each other, as shown in Fig. 1. Thus, the 0° and 90° polarizers correspond to $-\pi/4$ and $\pi/4$ in Fig. 2(a).

B. Pixel Characteristics

1) Sensitivity Spectrum: Fig. 5 shows the result of the spectral sensitivity measurement. The photodiode in the pixel comprised the n-well/p-sub structure of the standard CMOS process. The measured sensitivity peak was at approximately 750 nm. In the electric-field measurement demonstrated in Section IV, a ZnTe crystal is typically used as a probe.

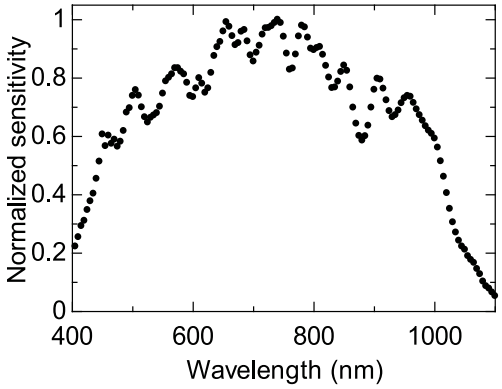

Fig. 5. Sensitivity spectrum of the pixel.

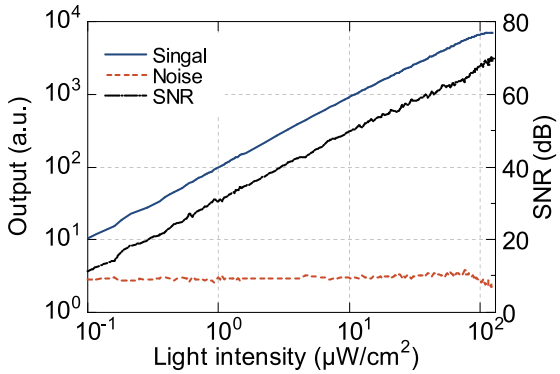

Fig. 6. Signal, noise and signal-to-noise ratio of the pixel. The exposure time was 100 ms.

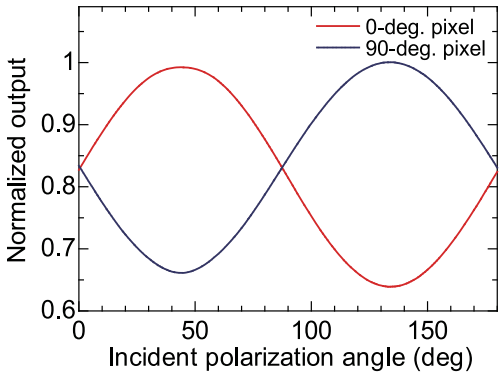

Fig. 7. Normalized output versus incident polarization angle.

In this case, a near-infrared wavelength band with a sufficiently high optical transmission of the ZnTe crystal is required. In this experiment, we confirmed that the sensor exhibited high sensitivity in this wavelength band.

2) Signal-to-Noise Ratio: To measure a small change in polarization, a high SNR is required. The output signal as a function of incident light intensity was measured. In addition, the standard deviation of the signal output was measured as the temporal noise. The result is shown in Fig. 6.

From the measurement results, the maximum SNR was approximately 63 dB. This indicates that it is possible to detect fluctuations of less than 0.1% under appropriate light intensity conditions. The full well capacity was approximately 8 Me^-.

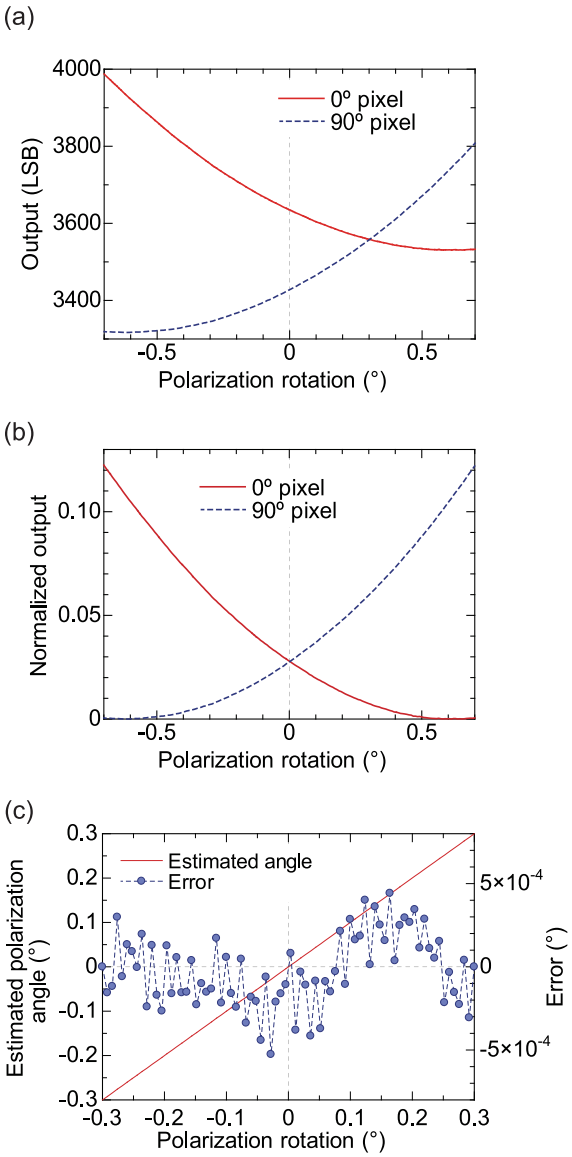

Fig. 8. (a) Measured output of 0° and 90° pixels as a function of incident light polarization rotation. (b) Normalized output version of (a), (c) Estimated polarization angle and error versus polarization rotation angle.

3) Polarization Extinction Ratio: To confirm the extinction ratio of the ON-pixel polarizer, we irradiated the fabricated sensor with linearly polarized light and measured the output as the polarization angle was rotated. The normalized outputs are plotted in Fig. 7. The wavelength of the irradiated light was 625 nm. The outputs are complementary to each other, indicating that the wire grids on the pixels act as polarizers. The extinction ratio was 1.55 for the 0° pixel and 1.53 for the 90° pixel. Although the grating line and space are identical in the design, there is a slight difference in output. This could be due to the slight difference in the fabricated structure from the design but further investigation is required. A correction is required to reduce this difference and improve measurement accuracy.

4) Sensitivity to Polarization Angle Modulation: In our proposed polarizer configuration, two polarizers were stacked to achieve a high polarization angle resolution. In this

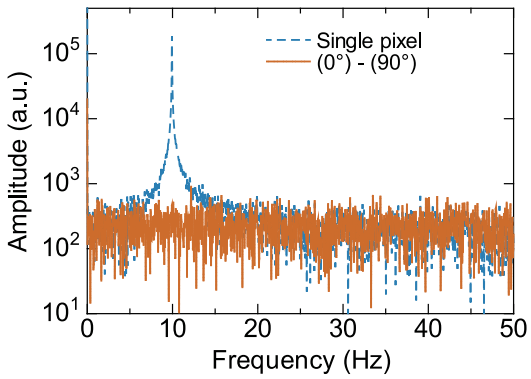

Fig. 9. Signal spectra of single pixel output and difference between 0° and 90° pixels when modulated light is irradiated.

experiment, a film polarizer was used as an external polarizer (SHLP41, MeCan imaging). The polarization image sensor chip was mounted using the following method. We first irradiated linearly polarized light, adjusted the polarization angle so that the outputs of the 0° and 90° polarizer-mounted pixels were the same, and then placed an external polarizer so that the transmittance was minimized.

To evaluate the polarization angle detection performance, a 625-nm light-emitting diode (LED) was used as the light source. The light irradiated on the stacked polarizer device was linearly polarized by passing it through a polarizer (LPVIS100-MP2, Thorlabs) with an extinction ratio of approximately 10^6. Fig. 8(a) shows the averaged values of the output of each polarizer-equipped pixel. The 96 frames of 50×50 pixels were averaged. Although asymmetric, the minima of both are approximately at $\pm 0.6°$. In addition, the output signal range in this measurement range was approximately 500 LSB, whereas the offset was approximately 3300–3500 LSB. This large offset is due to the low extinction ratio of the polarizer on the pixel. Fig. 8(b) shows the output normalized by the extinction ratio measurement results. The normalized outputs are symmetrical with respect to 0°, which is the lowest transmittance point of the external polarizer. Fig. 8(c) shows the result of taking the difference between these results and estimating the angle change from the pixel output. The blue dotted line indicates the error from the ideal value. The results show that the maximum error is $5.2 \times 10^{-4}°$, in the range of $\pm 0.3°$.

5) Common Mode Rejection: In the proposed method, pixels equipped with mutually orthogonal polarizers are placed next to each other on the pixel array. Then, as shown in Figs. 2(b) and 8(c), a signal proportional to the amount of polarization rotation can be obtained by subtracting their outputs. In this method, common-mode noise can be reduced. The common mode is superimposed on the detection signal when the light source intensity fluctuates. Thus, the ability to cancel this noise is expected to enable more sensitive polarization modulation detection.

To confirm this, we obtained the spectrum of the pixel output signal acquired by irradiating the modulated light; the results are presented in Fig. 9. It was irradiated with light modulated by a sinusoidal wave with a frequency of 10 Hz and an amplitude of 10% and measured at a frame rate of

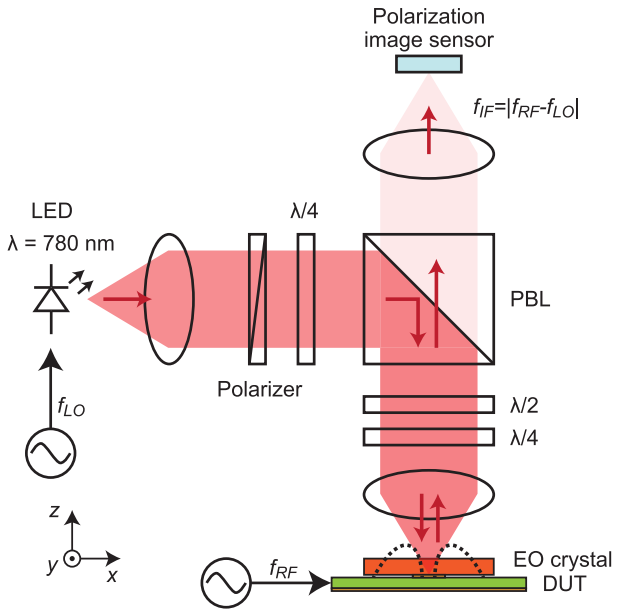

Fig. 10. Experimental setup of RF electric-field imaging. PBL is a polarization beam splitter.

100 fps. The output from a single pixel shows a sharp peak at 10 Hz owing to the light modulation. The orange line is the spectrum of the signal difference between neighboring pixels with different polarizer directions. This result indicates that the common-mode component is canceled by taking the difference and can be reduced to a noise level or less.

IV. Imaging Demonstration

One of the advantages of the proposed image sensor is that it can detect weak polarization changes in an image. In this study, we demonstrate electric-field imaging based on the Pockels effect, which is a first-order EO effect. Because of this effect, an EO crystal exhibits birefringence index changes. Therefore, the polarization state of the transmitted light is changed by the application of an electric field [18], [19]. Its refractive index change is given by

$$\Delta n = \pm \frac{1}{2} n^3 r_{\text{eff}} E \tag{3}$$

where n is the refractive index of the crystal and r_{eff} is the effective Pockels coefficient, which depends on the Pockels coefficient of the crystal, the direction of the electric field, and the direction of propagation and polarization of the light, where E denotes the electric field.

Highly sensitive polarization-modulation detection is required when observing minute electric-field changes. Real-time imaging using an image sensor has been demonstrated so far; however, its sensitivity is lower than that of a single detection system [15], [20].

To perform electric-field imaging using the fabricated polarization image sensor, we constructed the system shown in Fig. 10. In this system, an optical heterodyne method is used because the frame rate of the image sensor is much lower than that of the high-frequency electric field. The light modulated by the local oscillation frequency f_{LO} is irradiated to the electric-field signal at a frequency f_{RF} of the observation target

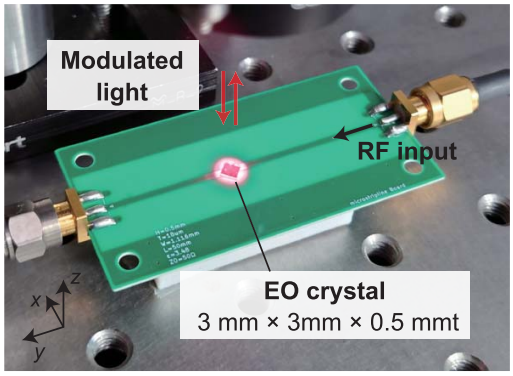

Fig. 11. Photograph of the DUT under electric-field imaging.

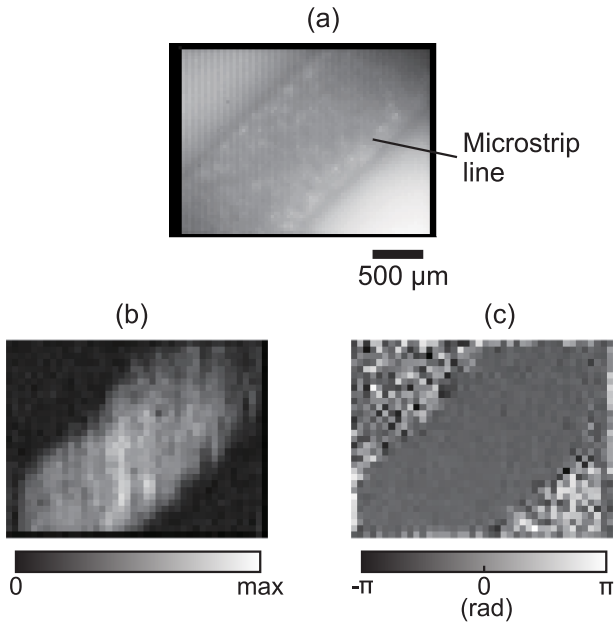

Fig. 12. (a) Optical image of the DUT by the polarization image sensor. Electric-field images of (b) amplitude and (c) phase.

and the intermediate frequency component $f_{\text{IF}} = |f_{\text{RF}} - f_{\text{LO}}|$ is generated by mixing in the EO crystal. The polarization image sensor acquires images of intermediate frequency. The intermediate frequency is set to an integer fraction of the frame rate and the intensity and phase images of the electric field can be obtained by calculating the amplitude and phase from the acquired data.

In this study, (100)-ZnTe was used as the EO crystal. This provides polarization modulation for the electric field in the z-direction in Figs. 10 and 11. The top and bottom surfaces of the EO crystal were coated with anti-reflection (AR) and high-reflection coatings at 780 nm, respectively. The light source used for observation was an infrared LED (M780L3, Thorlabs), with a peak wavelength of 780 nm.

A microstrip line was used for the device under test (DUT). The substrate of the DUT was FR-4. The linewidth was 1.1 mm and it was designed to have a characteristic impedance of approximately 50 Ω.

Fig. 11 shows a photograph of the device-under-test (DUT) during the experiment. The EO crystal ((100)-ZnTe, 3 mm × 3 mm × 0.5 mm) was placed directly on the DUT,

the modulated light was irradiated and the reflected light was observed. The red area in the figure was irradiated with modulated light from above and the light was reflected back to the HR coating on the bottom of the crystal. The f_{RF} and amplitude of the electric-field signal input to the DUT were 100.005 kHz and 5 V, respectively, and the modulation frequency f_{LO} of the LED was set to 100 kHz. The image sensor cannot directly observe the high-frequency signal. However, the signal at the intermediate frequency of 5 Hz can be detected. The signal also contains information on the electric-field distribution of the high-frequency signal at f_{RF} to the DUT, which is the target of observation. In this experiment, 16 384 frames were acquired at a frame rate of 100 fps. The signal intensity and phase of the relevant frequency components were obtained by Fourier transform after subtracting the difference between adjacent pixels with ON-pixel polarizer angles orthogonal to each other.

The imaging results of the image sensor are shown in Fig. 12. Fig. 12(a) shows an optical image without the EO crystal, showing the observation area on the DUT. It can be seen that there is a microstrip line in the diagonal direction of the observation area. Fig. 12(b) shows the amplitude distribution of the signal component at frequency f_{IF} and Fig. 12(c) shows the phase distribution. The amplitude distribution image shows that the signal amplitude is higher on the microstrip line. In addition, the phase was almost constant along the line because the (100)-ZnTe crystal detects the signal of the electric field spreading upward from the microstrip line, which is the z-direction in Fig. 10(a) [21]. In addition, using a (110)-ZnTe crystal, the electric-field components in parallel in the x- or y-directions can be imaged.

V. Discussions

A. ON-Chip Polarizers

The 0.35-μm process was used in this project and, unlike in the case of the nanostructure, the metal grid polarizer has a difference in polarization transmittance because of the difference in diffraction efficiency. As a result, the pixel extinction ratio was as low as 1.55. In contrast, polarizers with a nanoscale metal grid structure using a 65-nm process have achieved extinction ratios of up to approximately 100 [13]. This result is comparable to that reported for similar structures in other groups [22], [23]. However, as shown in Fig. 2(c), when the ON-pixel polarizers are used as optical analyzers, the relative sensitivity exceeds the theoretical limit of 80% at approximately 10 of the extinction ratio. This value can be achieved using a relatively mature CMOS process. Therefore, it is expected that high performance can be achieved without exploiting the ultrafine polarizer process.

In the electric filed imaging demonstration, we used an external high-extinction polarizer or polarization beam splitter as the first polarization layer. It is possible to integrate it on the chip. However, a special process should be used to achieve a sufficient extinction ratio of more than a few hundred.

B. Signal-to-Noise Ratio

In the proposed method, the polarization rotation angle is enhanced by an external polarizer to improve the detection angle. However, it is also important to increase the SNR of the pixel itself because there is a limit to the light source intensity that can be practically used. The maximum SNR of the pixels in this study was 63 dB. However, noise factors other than photon-shot noise were dominant. The pixel architecture is a 3-transistor active pixel sensor. Thus, there is room for improvement by introducing a 4-transistor active pixel sensor with a correlated double sampling (CDS) circuit to reduce kTC noise.

To improve the effective extinction ratio, it is important to increase the performance of the on-pixel polarizer itself, as well as the crosstalk between pixels. In a standard CMOS process, the spacing between the PDs must be increased to reduce crosstalk. Thus, there is potential to make the circuit configuration per pixel more complex. This strategy can increase the effective pixel capacitance and improve the SNR using a self-resetting circuit [24], [25] or a self-resetting circuit [26]–[28]. In the case of high spatial resolution, techniques for reducing crosstalk, such as a vertical waveguide structure and deep trench isolation, are required.

C. Application to High-Frequency Electric-Field Imaging

In this study, we demonstrated visualizing the electric field on a microstrip line via a fabricated polarization image sensor. The input frequency was set to 100.005 kHz. This was due to the modulation frequency limit of the light source used in this study. EO crystals (ZnTe) are responsive to high frequencies up to the THz range and have been used for microwave, millimeter-wave [20], [29], and THz field imaging [30], [31]. In conjunction with a modulated light that can respond to these frequency bands, it should be possible to observe higher frequencies.

VI. Conclusion

A prototype image sensor was fabricated, with ON-chip polarizers in mutually orthogonal directions between adjacent pixels. It was shown that a stacked polarizer structure could achieve high sensitivity and linearity for detecting polarization changes. The noise level was $5.2 \times 10^{-4\circ}$ for a light source of 625 nm and 96 frames of 50×50 pixels. The proposed method enables the detection of weak changes in polarization that ordinary polarization image sensors cannot detect. As an application example, we demonstrated high-frequency electric-field imaging using the EO effect. We showed that highly sensitive polarization-modulation imaging could be used to acquire weak changes in parallel, which can typically only be obtained by a single-point measurement. In this example, the acquired data were processed using post-processing software. However, it is expected that constructing a real-time processing system will allow special imaging based on optical polarization.

References

[1] G. A. Atkinson and E. R. Hancock, "Recovery of surface orientation from diffuse polarization," *IEEE Trans. Image Process.*, vol. 15, no. 6, pp. 1653–1664, Jun. 2006, doi: 10.1109/TIP.2006.871114.

[2] S.-S. Lin, K. M. Yemelyanov, E. N. Pugh, and N. Engheta, "Polarization-based and specular-reflection-based noncontact latent fingerprint imaging and lifting," *J. Opt. Soc. Amer. A, Opt. Image Sci.*, vol. 23, no. 9, pp. 2137–2153, Sep. 2006, doi: 10.1364/JOSAA.23.002137.

[3] N. A. Rubin, G. D'Aversa, P. Chevalier, Z. Shi, W. T. Chen, and F. Capasso, "Matrix Fourier optics enables a compact full-Stokes polarization camera," *Science*, vol. 365, no. 6448, pp. 1–10, Jul. 2019, doi: 10.1126/science.aax1839.

[4] V. Gruev, J. Van der Spiegel, and N. Engheta, "Dual-tier thin film polymer polarization imaging sensor," *Opt. Exp.*, vol. 18, no. 18, pp. 19292–19303, Aug. 2010, doi: 10.1364/OE.18.019292.

[5] X. Zhao, A. Bermak, F. Boussaid, and V. G. Chigrinov, "Liquid-crystal micropolarimeter array for full Stokes polarization imaging in visible spectrum," *Opt. Exp.*, vol. 18, no. 17, pp. 17776–17787, Aug. 2010, doi: 10.1364/OE.18.017776.

[6] T. Sato, T. Araki, Y. Sasaki, T. Tsuru, T. Tadokoro, and S. Kawakami, "Compact ellipsometer employing a static polarimeter module with arrayed polarizer and wave-plate elements," *Appl. Opt.*, vol. 46, no. 22, pp. 4963–4967, 2007, doi: 10.1364/AO.46.004963.

[7] T. Tokuda, S. Sato, H. Yamada, K. Sasagawa, and J. Ohta, "Polarisation-analysing CMOS photosensor with monolithically embedded wire grid polariser," *Electron. Lett.*, vol. 45, no. 4, pp. 228–230, 2009, doi: 10.1049/EL:20093132.

[8] T. Tokuda, H. Yamada, K. Sasagawa, and J. Ohta, "Polarization-analyzing CMOS image sensor with monolithically embedded polarizer for microchemistry systems," *IEEE Trans. Biomed. Circuits Syst.*, vol. 3, no. 5, pp. 259–266, Oct. 2009, doi: 10.1109/TBCAS.2009.2022835.

[9] V. Gruev, R. Perkins, and T. York, "CCD polarization imaging sensor with aluminum nanowire optical filters," *Opt. Exp.*, vol. 18, no. 18, pp. 19087–19094, Aug. 2010, doi: 10.1364/OE.18.019087.

[10] M. Sarkar, D. S. S. S. S. Bello, C. van Hoof, and A. Theuwissen, "Integrated polarization analyzing CMOS image sensor for material classification," *IEEE Sensors J.*, vol. 11, no. 8, pp. 1692–1703, Aug. 2011, doi: 10.1109/JSEN.2010.2095003.

[11] S. Shishido, T. Noda, K. Sasagawa, T. Tokuda, and J. Ohta, "Polarization analyzing image sensor with on-chip metal wire grid polarizer in 65-nm standard complementary metal oxide semiconductor process," *Jpn. J. Appl. Phys.*, vol. 50, no. 4, Apr. 2011, Art. no. 04DL01, doi: 10.1143/JJAP.50.04DL01.

[12] M. Sarkar, D. S. S. Bello, C. van Hoof, and A. J. P. Theuwissen, "Biologically inspired CMOS image sensor for fast motion and polarization detection," *IEEE Sensors J.*, vol. 13, no. 3, pp. 1065–1073, Mar. 2013, doi: 10.1109/JSEN.2012.2234101.

[13] K. Sasagawa *et al.*, "Image sensor pixel with on-chip high extinction ratio polarizer based on 65-nm standard CMOS technology," *Opt. Exp.*, vol. 21, no. 9, pp. 11132–11140, 2013, doi: 10.1364/OE.21.011132.

[14] M. Zhang, X. Wu, N. Cui, N. Engheta, and J. Van der Spiegel, "Bioinspired focal-plane polarization image sensor design: From application to implementation," *Proc. IEEE*, vol. 102, no. 10, pp. 1435–1449, Oct. 2014, doi: 10.1109/JPROC.2014.2347351.

[15] K. Sasagawa, A. Kanno, T. Kawanishi, and M. Tsuchiya, "Live electrooptic imaging system based on ultraparallel photonic heterodyne for microwave near-fields," *IEEE Trans. Microw. Theory Techn.*, vol. 55, no. 12, pp. 2782–2791, Dec. 2007, doi: 10.1109/TMTT.2007.909889.

[16] K. Sasagawa, A. Kanno, and M. Tsuchiya, "Real-time digital signal processing for live electro-optic imaging," *Opt. Exp.*, vol. 17, no. 18, pp. 15641–15651, Aug. 2009, doi: 10.1364/OE.17.015641.

[17] R. Okada, K. Sasagawa, M. Haruta, H. Takehara, H. Tashiro, and J. Ohta, "A polarisation-analysing CMOS image sensor for sensitive polarisation modulation detection," *Electron. Lett.*, vol. 57, no. 12, pp. 472–474, Jun. 2021, doi: 10.1049/ell2.12169.

[18] K. Yang, G. David, S. V. Robertson, J. F. Whitaker, and L. P. B. Katehi, "Electrooptic mapping of near-field distributions in integrated microwave circuits," *IEEE Trans. Microw. Theory Techn.*, vol. 46, no. 12, pp. 2338–2343, Dec. 1998, doi: 10.1109/22.739221.

[19] D.-J. Lee and J. F. Whitaker, "An optical-fiber-scale electro-optic probe for minimally invasive high-frequency field sensing," *Opt. Exp.*, vol. 16, no. 26, pp. 21587–21597, Dec. 2008, doi: 10.1364/OE.16.021587.

[20] M. Tsuchiya, K. Sasagawa, A. Kanno, and T. Shiozawa, "Live electrooptic imaging of *W*-band waves," *IEEE Trans. Microw. Theory Techn.*, vol. 58, no. 11, pp. 3011–3021, Nov. 2010, doi: 10.1109/TMTT.2010.2076672.

[21] L. Duvillaret, S. Rialland, and J. Coutaz, "Electro-optic sensors for electric field measurements. II. Choice of the crystals and complete optimization of their orientation," *J. Opt. Soc. Amer. B, Opt. Phys.*, vol. 19, no. 11, pp. 2704–2715, 2002, doi: 10.1364/JOSAB.19.002704.

[22] T. Yamazaki *et al.*, "Four-directional pixel-wise polarization CMOS image sensor using air-gap wire grid on 2.5-μm back-illuminated pixels," in *IEDM Tech. Dig.*, Dec. 2016, p. 8, doi: 10.1109/IEDM.2016.7838378.

[23] Y. Maruyama *et al.*, "3.2-MP back-illuminated polarization image sensor with four-directional air-gap wire grid and 2.5-μm pixels," *IEEE Trans. Electron Devices*, vol. 65, no. 6, pp. 2544–2551, May 2018, doi: 10.1109/TED.2018.2829190.

[24] Y. Fujihara *et al.*, "A multi spectral imaging system with a 71 dB SNR 190–1100 nm CMOS image sensor and an electrically tunable multi bandpass filter," *ITE Trans. Media Technol. Appl.*, vol. 6, no. 3, pp. 187–194, 2018, doi: 10.3169/MTA.6.187.

[25] M. Murata *et al.*, "A high near-infrared sensitivity over 70-dB SNR CMOS image sensor with lateral overflow integration trench capacitor," *IEEE Trans. Electron Devices*, vol. 67, no. 4, pp. 1653–1659, Apr. 2020, doi: 10.1109/TED.2020.2975602.

[26] K. Sasagawa *et al.*, "An implantable CMOS image sensor with self-reset pixels for functional brain imaging," *IEEE Trans. Electron Devices*, vol. 63, no. 1, pp. 215–222, Jan. 2016, doi: 10.1109/TED.2015.2454435.

[27] T. Yamaguchi *et al.*, "Implantable self-reset CMOS image sensor and its application to hemodynamic response detection in living mouse brain," *Jpn. J. Appl. Phys.*, vol. 55, no. 4S, Apr. 2016, Art. no. 04EM02, doi: 10.7567/JJAP.55.04EM02.

[28] T. Pakpuwadon *et al.*, "Self-reset image sensor with a signal-to-noise ratio over 70 dB and its application to brain surface imaging," *Frontiers Neurosci.*, vol. 15, Jun. 2021, Art. no. 667932, doi: 10.3389/fnins.2021.667932.

[29] A. I. Sasaki and T. Nagatsuma, "Millimeter-wave imaging using an electrooptic detector as a harmonic mixer," *IEEE J. Sel. Topics Quantum Electron.*, vol. 6, no. 5, pp. 735–740, Sep./Oct. 2000, doi: 10.1109/2944.892612.

[30] Q. Wu, T. D. Hewitt, and X.-C. Zhang, "Two-dimensional electro-optic imaging of THz beams," *Appl. Phys. Lett.*, vol. 69, no. 8, pp. 1026–1028, Aug. 1996, doi: 10.1063/1.116920.

[31] Q. Chen, M. Tani, Z. Jiang, and X.-C. Zhang, "Electro-optic transceivers for terahertz-wave applications," *J. Opt. Soc. Amer. B, Opt. Phys.*, vol. 18, no. 6, pp. 823–831, Jun. 2001, doi: 10.1364/JOSAB.18.000823.